Hindawi
Wireless Communications and Mobile Computing
Volume 2020, Article ID 8853794, 7 pages
https://doi.org/10.1155/2020/8853794

Research Article

Beam Pattern Optimization Method for Subarray-Based Hybrid Beamforming Systems

Joerg Eisenbeis, Jonas Pfaff, Christian Karg, Jerzy Kowalewski, Yueheng Li, Mario Pauli, and Thomas Zwick

Institute of Radio Frequency Engineering and Electronics (IHE), Karlsruhe Institute of Technology (KIT), Kaiserstr. 12, 76131 Karlsruhe, Germany

Correspondence should be addressed to Joerg Eisenbeis; joerg.eisenbeis@kit.edu

Received 30 July 2020; Revised 22 November 2020; Accepted 14 December 2020; Published 28 December 2020

Academic Editor: Luis Castedo

Massive multiple-input multiple-output (MIMO) systems operating at millimeter-wave (mmWave) frequencies promise to satisfy the demand for higher data rates in mobile communication networks. A practical challenge that arises is the calibration in amplitude and phase of these massive MIMO systems, as the antenna elements are too densely packed to provide a separate calibration branch for measuring them independently. Over-the-air (OTA) calibration methods are viable solutions to this problem. In contrast to previous works, the here presented OTA calibration method is investigated and optimized for subarray-based hybrid beamforming (SBHB) systems. SBHB systems represent an efficient architectural solution to realize massive MIMO systems. Moreover, based on OTA scattering parameter measurements, the ambiguities of the phase shifters are exploited and two criteria to optimize the beam pattern are formulated. Finally, the optimization criteria are examined in measurements utilizing a novel SBHB receiver system operating at 27.8 GHz.

1. Introduction

Massive multiple-input multiple-output (MIMO) systems operating in the centimeter-wave (cmWave) and millimeter-wave (mmWave) regions are considered for the further expansion of mobile communication networks [1–4]. Those massive MIMO systems can achieve huge spectral efficiencies by exploiting the multipath wireless channel [5]. However, fully digital MIMO architectures consist of a separate transceiver for each antenna element, which makes them expensive and energy-hungry [6, 7]. An efficient architectural solution is the concept of hybrid beamforming systems, separating the beamforming process into a digital part of reduced size in combination with an analog beamforming network [8–10]. These hybrid beamforming systems reduce the number of digital channels, i.e., the number of digital-to-analog and analog-to-digital converters (DACs/ADCs), while conserving precise beamforming employing an analog beamforming network. A low-complex architectural realization of the analog beamforming network is the subarray-based (also denominated as *subconnected* or *partially connected*) hybrid beamforming (SBHB) architecture [11–13]. The SBHB architecture connects each digital channel to a subarray of antenna elements via a dedicated phase shifter.

To steer the antenna beam into the desired direction and to generate the desired beam pattern, a calibration in amplitude and phase of the different radio frequency (RF) branches is required [14]. This functionality is crucial for currently investigated channel estimation and beamforming algorithms [15–22]. To tackle the calibration problem over-the-air (OTA) calibration methods seem to be promising, as no additional RF calibration branches have to be integrated into the analog beamforming network. Note that a RF calibration branch per antenna element is technically and economically challenging, as massive MIMO arrays consist of hundreds of densely packed antenna elements [23, 24]. The presented OTA method in [25] for retrodirective antenna arrays calibrates the phases of the elements regarding a reference transmitter. This allows precise beam steering towards the reference but does not calibrate the amplitude and phase

imbalances between the RF branches. Another OTA approach is shown in [26], where the OTA calibration is performed using the equivalent current technique with a spherical near-field multiprobe system. Nevertheless, the utilized measurement system is limited to 18 GHz, and the size of the measured object is constrained. In [27], the amplitude and phase of a phased array system are calibrated by performing OTA scattering parameter measurements.

This work presents an OTA calibration method for SBHB systems based on scattering parameter measurements. To verify the calibration, a novel SBHB receiver system operating at 27.8 GHz is developed. In the first step, successive OTA measurements of the complex transmission coefficient between a reference transmitter and each receive antenna are performed. The comparison between measurements allows calibration of the relative amplitude and phase difference between the RF chains at the receiver. In contrast to [27], the beam patterns are further optimized by exploiting the ambiguities of the phase shifters. To optimally exploit the phase shifter ambiguities, two optimization criteria are formulated and verified by conducting beam pattern measurements. The presented results indicate a clear performance improvement by selecting the phase shifter states optimizing the transmission gain.

This paper is structured as follows. First, the developed SBHB receiver is presented in Section 1. Subsequently, the OTA calibration method is discussed in Section 2, including the required measurement setup and calibration result. Finally, in Section 3, two optimization criteria are proposed and evaluated in measurements exploiting the phase shifter ambiguities to further improve the antenna beam pattern.

2. Subarray-Based Hybrid Beamforming Receiver

The overall receiver system consists of an independent antenna board, a SBHB receiver backend module, and two software-defined radios (SDRs). This modular setup enables characterizing the SBHB receiver independently and allows future changes like the testing of different antenna concepts. A block diagram of the receiver system is shown in Figure 1. The SBHB receiver connects $N_{\text{sub}} = 4$ receive antennas to one digital channel creating $N_{\text{dig}} = 4$ independent subarrays. The antenna board, designed in a previous study [28], consists of a uniform linear microstrip patch antenna array with $N_{\text{ant}} = 16$ elements arranged in the horizontal plane. The element spacing is $\lambda_0/2 \approx 5.35$ mm, where λ_0 represents the wavelengths at 27.8 GHz. To improve the antenna element gain, two serially fed microstrip patch elements are vertically stacked, narrowing down the half-power beamwidth (HPBW) in elevation direction to 40.8°. The HPBW in azimuth is 86°, and the measured realized element gain, including the connector and feed line losses, is 4 dBi. The SBHB receiver combines four antenna elements to one digital channel as shown in Figure 1.

A system on a chip (SoC) by Anokiwave of type *AWMF-0108* [29] with four input channels and one output channel represents the core of the SBHB receiver. Each of the four

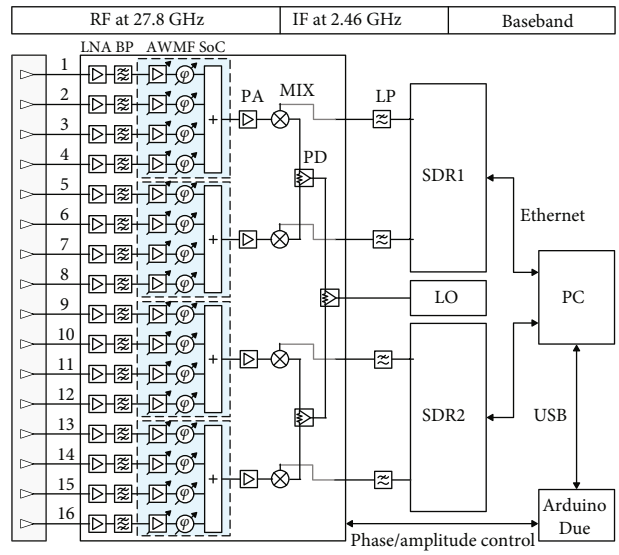

Figure 1: Block diagram of the SBHB receiver system including a photo of the SBHB receiver frontend.

input channels of the *AWMF-0108* consists of a phase shifter and digital attenuator with a 5-bit resolution each. The branches are then connected via a power combiner on the *AWMF-0108* SoC. The digital attenuators and phase shifters of the *AWMF-0108* are controlled via a serial peripheral interface (SPI) using an Arduino Due microcontroller. A software interface is implemented onto the microcontroller translating the desired phase and attenuation settings defined by a host computer into the required code sequence to control the *AWMF-0108* SoC. This software interface also enables to define an offset vector between the phase and amplitude states of the RF branches, which are utilized to take into account the calibration carried out later. Furthermore, a switch-off function for each RF branch is implemented by controlling the power supply of the first low noise amplifier (LNA) after the antenna element and setting the digital attenuator within the *AWMF-0108* SoC to its maximum value. After combining the four input channels, the received signal is further amplified and downconverted from the RF at 27.8 GHz to an intermediate frequency (IF) at 2.46 GHz. The required local oscillator (LO) signal for downconversion is provided externally at half the LO frequency, i.e., 12.67 GHz.

The antenna board, as well as the SBHB receiver, is designed using a four-layer printed circuit board (PCB) with a *RO4003C* substrate of 200 μm thickness and a dielectric constant of $\varepsilon_r = 3.38$ from Rogers Corporation. For electromagnetic shielding, protection, and better heat dissipation, the SBHB receiver is integrated into a metallic housing. Each amplifier stage is enclosed in a metallic chamber, which is lined with absorber material of type *ECCOSORB GDS* from Laird Performance Materials. Finally, the four IF outputs of the SBHB receiver are connected to two SDRs. The SDRs perform IF signal processing, downconversion, and analog-to-digital conversion. As SDRs, we employ the commercially available platforms provided by Ettus Research LLC, i.e.,

universal software radio peripherals (USRPs) of type *X310*. A photo of the SBHB receiver is shown in Figure 2.

3. OTA Calibration Method

In general, the parallel RF branches in the analog beamforming network of the SBHB systems are prone to amplitude and phase differences, caused by nonideal circuit board manufacturing, deviations between the used integrated circuits, connectors, and soldering tolerances. In particular, the phase imbalances between the RF branches are more pronounced at higher frequencies due to the low wavelength, which leads to strong phase differences caused by small line length differences. As a result, a precise calibration between the parallel RF branches is required. This calibration becomes challenging as in massive MIMO systems several hundreds of antennas are closely packed. Classical outcoupling of a part of the receive or transmit power close to the antenna is technically challenging and inefficient, as it requires a huge number of feedback branches [23]. As a consequence, this work focuses on OTA calibration methods. To correct phase and amplitude imbalances between the RF branches, digital phase shifters and digital attenuators are utilized provided by the *AWMF-0108* SoC. This means that the achievable accuracy of the calibration is limited by the phase shifter and digital attenuator resolution. For the OTA calibration, the measurement setup presented in Figure 3 is utilized. The setup is aimed at measuring the complex transmission coefficients, namely, S_{21}, between a reference transmitter and each receiver of the SBHB system. Therefore, the transmitter and SBHB receiver are separated by 6 m and ideally aligned in an anechoic chamber. A photo of the SBHB receiver in the anechoic chamber is shown in Figure 2. At the transmitter side, a mixer of the same type as used for the SBHB receiver is employed in combination with a quad ridged horn antenna from RFspin Ltd. of type *QRH40* offering 14 dBi antenna gain and a half-power beamwidth (HPBW) of 27.8° at the selected center frequency $f_{RF} = 27.8$ GHz. To enable a measurement of the complex transmission factor, the local oscillator signal for IF to RF up- and down-conversion is provided by the same signal generator. Moreover, the utilized vector network analyzer (VNA) from Keysight Technologies of type *N9952A* is operated at the IF frequency band from 1.26 GHz to 3.66 GHz resulting to a RF frequency band between 26.6 GHz and 29 GHz. The VNA is synchronized with the signal generator via a 10 MHz reference signal. The transmit power is selected to $P_{\mathrm{Tx}} = -17$ dBm resulting in a received power of $P_{\mathrm{Rx}} = -76$ dBm with a FSPL = 77 dB at 27.8 GHz.

With the presented measurement setup, the complex transmission matrix $\mathbf{S} \in \mathbb{C}^{N_q \times N_{\mathrm{ant}}}$ can be measured for all N_{ant} receive antennas and for all $N_q = 2^q$ phase shifter states, where q represents the resolution of the utilized digital phase shifter. The digital attenuators are set to their minimum for all branches to increase the receive signal-to-noise ratio (SNR). The measurements between the reference transmitter and each receiver branch of a subarray are performed subsequently in an automated process. The 32 possible phase

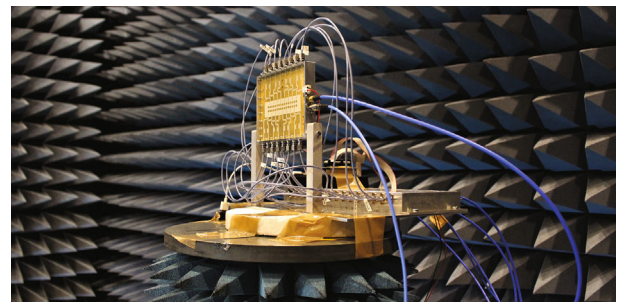

Figure 2: Photo of the SBHB receiver system.

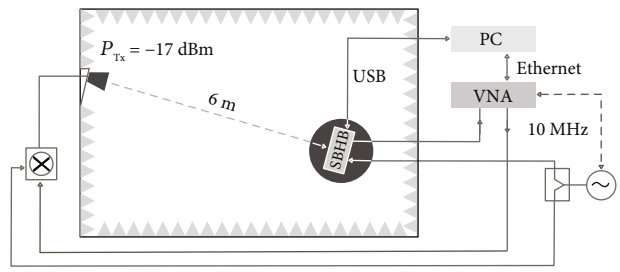

Figure 3: Measurement setup for OTA calibration.

shifter states multiplied by the 16 RF branches result in a total of 512 measurements. Each measurement depends on the number of points in the frequency domain, the selected resolution bandwidth, and the selected averaging factor. For the selected 301 measurement points in the frequency domain, the resolution bandwidth of 10 kHz, and an averaging over 20 measurements, yields an overall measurement time per subarray of approximately 1.5 h. As the phase and amplitude differences between the subarrays can be corrected in the digital domain, only the imbalances between the N_{sub} antenna elements of a subarray must be compensated. Therefore, we reformulate the complex transmission matrix to $\mathbf{S} = [\mathbf{S}_1, \cdots, \mathbf{S}_{N_{\mathrm{dig}}}]$, where the transmission matrix of the dth subarray has the shape $S_d \in \mathbb{C}^{N_q \times N_{\mathrm{sub}}}$ for all $d \in \{1, \cdots, N_{\mathrm{dig}}\}$. The measured phase of the transmission matrix $\angle\mathbf{S}$ is presented in Figure 4(a). It can be observed that large phase imbalances exist between the different RF branches. The measurement results also show a deviation from the desired phase difference between the phase shifter states of the individual branches. Based on the measured transmission matrix, the calibration vector for each subarray $\mathbf{c}_d = [c_{d,1}, \cdots, c_{d,N_{\mathrm{sub}}}]$ with $c_{d,i_s} \in \{1, \cdots, N_q\}$ for all $i_s \in \{1, \cdots, N_{\mathrm{sub}}\}$ subarray antenna elements can be determined.

This is done by finding the optimal calibration vector

$$\mathbf{c}_d^{\mathrm{opt}} = \arg \min_{\mathbf{c}_d} \left\{ \sum_{i_q=1}^{N_q} \sum_{i_s=1}^{N_{\mathrm{sub}}} \left| \angle \mathbf{S}_d(\hat{i}_q, i_s) - \frac{1}{N_{\mathrm{sub}}} \sum_{p=1}^{N_{\mathrm{sub}}} \angle \mathbf{S}_d(\hat{i}_q, p) \right| \right\}, \tag{1}$$

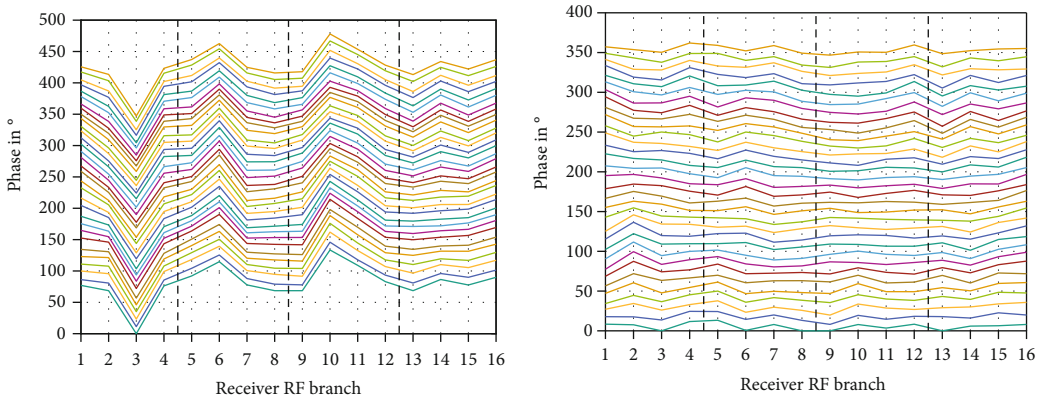

(a) Uncalibrated result (b) Calibrated result

Figure 4: Measured phase of the uncalibrated and calibrated transmission matrix **S** at 27.8 GHz.

Table 1: Phase error and mean CG of the proposed optimization criteria.

	RMS	$\zeta_\beta^{\text{ph,opt}}$	$\zeta_\beta^{\text{am,opt}}$
Phase error	7.0°	2.1°	6.3°
SBHB mean CG	45.2 dB	45.2 dB	47.6 dB

minimizing the phase differences between the RF branches of the dth subarray with

$$\hat{i}_q = \begin{cases} i_q + c_{d,i_s}, & i_q + c_{d,i_s} \le N_q, \\ i_q + c_{d,i_s} - N_q, & i_q + c_{d,i_s} > N_q. \end{cases} \tag{2}$$

The measurement result of the phase of the transmission matrix after applying the determined optimal calibration vector is shown in Figure 4(b). The average phase error could be reduced from 28.8° before calibration to 6.6° at 27.8 GHz. The average phase error stays below 12° within 690 MHz from 27.59 GHz to 28.28 GHz. The reduction of the phase error over a larger bandwidth can be further improved by utilizing a true-time delay phase shifter [30].

4. Optimized Beam Pattern by Phase State Selection

For the SBHB system, precise alignment of the beam in the desired spatial direction is crucial. The alignment of the individual subarrays is achieved, as in classical phased arrays, by setting a phase difference $\Delta\varphi$ between the RF branches. The adjustable phase difference depends on the resolution of the digital phase shifter. This results in the possible phase differences $\Delta\varphi = \beta\varphi_\delta$ with the minimal phase difference $\varphi_\delta = 2\pi/2^q$ and the differences of the phase shifter states β. The adjusted phase difference between the antenna elements results in a uniform linear array in steering towards [31]:

$$\phi = \arcsin\left\{\frac{\Delta\varphi}{kd_a}\right\}, \tag{3}$$

with the wave number $k = 2\pi/\lambda$ and the antenna element spacing d_a. The equation shows that only the relative phase between neighboring antenna elements is of importance to steer the beam into the desired direction. The possible phase shifter states $\beta \in \{-\beta_{\max}, \cdots, -1, 0, 1, \cdots, \beta_{\max}\}$ depend on the maximum desired steering angle $\phi_{\max}$ resulting to

$$\beta_{\max} = \lceil kd_a \sin\{\phi_{\max}\} \rceil. \tag{4}$$

As the beam steering into the desired angular direction can be achieved by N_q different phase shifter settings, this ambiguity can be exploited to further optimize the beam pattern. As the degree of freedom serves the phase index of the first antenna element $\zeta_\beta \in \{1, 2, \cdots, N_q\}$, which can be freely selected. The phases of all other antenna elements are then adjusted relative to the phase setting of the first antenna element.

One possibility is to select ζ_β leading to the minimum deviation between the desired phase difference $\beta\varphi_\delta$ and the actual phase difference between two adjacent branches. The optimization problem results in

$$\zeta_\beta^{\text{ph,opt}} = \arg\min_{\zeta_\beta}\left\{\sum_{i_s=1}^{N_{\text{sub}}}\left|\angle\mathbf{S}_d\left(i_{\zeta_\beta}^{i_s+1}, i_s+1\right) - \angle\mathbf{S}_d\left(i_{\zeta_\beta}^{i_s}, i_s\right) - \beta\varphi_\delta\right|\right\}, \tag{5}$$

where the indices are defined as

$$i_{\zeta_\beta}^{i_s+1} = \begin{cases} \zeta_\beta + c_{d,i_s+1}^{\text{opt}} + i_s\beta, & \zeta_\beta + c_{d,i_s+1}^{\text{opt}} + i_s\beta \le N_q, \\ \zeta_\beta + c_{d,i_s+1}^{\text{opt}} + i_s\beta - N_q, & \zeta_\beta + c_{d,i_s+1}^{\text{opt}} + i_s\beta > N_q, \end{cases} \tag{6}$$

$$i_{\zeta_\beta}^{i_s} = \begin{cases} \zeta_\beta + c_{d,i_s}^{\text{opt}} + (i_s-1)\beta, & \zeta_\beta + c_{d,i_s+1}^{\text{opt}} + (i_s-1)\beta \le N_q, \\ \zeta_\beta + c_{d,i_s}^{\text{opt}} + (i_s-1)\beta - N_q, & \zeta_\beta + c_{d,i_s+1}^{\text{opt}} + (i_s-1)\beta > N_q. \end{cases} \tag{7}$$

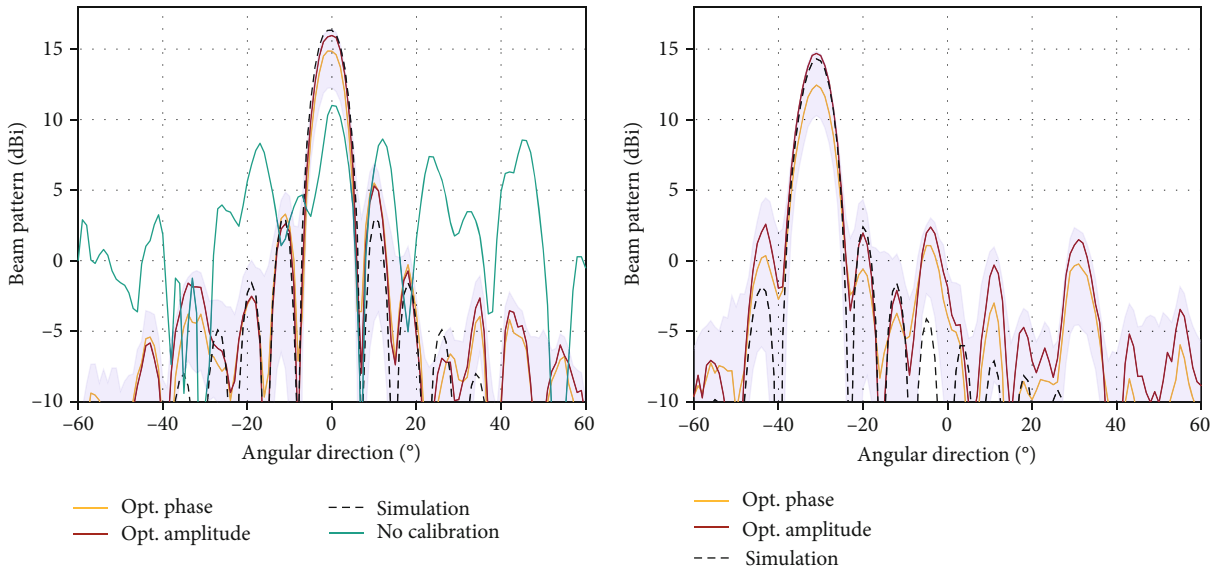

(a) Beam steering towards $\phi = 0°$

(b) Beam steering towards $\phi = -34°$

Figure 5: Beam pattern of the complete antenna array for the different optimization criteria.

Another possibility is to select ζ_β maximizing the mean conversion gain (CG) over all branches. The optimization problem therefore results in

$$\zeta_\beta^{\text{am,opt}} = \arg \min_{\zeta_\beta} \left\{ \sum_{i_s=1}^{N_{\text{sub}}} \left| \mathbf{S}_d \left(i_{\zeta_\beta}^{i_s}, i_s \right) \right| \right\}. \tag{8}$$

The changes of the phase error and the mean CG averaged over all possible angular directions are given in Table 1. As reference serves the root-mean-square (RMS) value over all phase indices ζ_β for both criteria. The results show that for $\zeta_\beta^{\text{ph,opt}}$, the phase error could be reduced to 2.1°, while the mean CG is identical to the RMS value. For $\zeta_\beta^{\text{am,opt}}$, the mean CG could be increased by 2.4 dB compared to the RMS value, while at the same time, the phase error is slightly improved compared to the reference.

As the phase error is sufficiently low to achieve a directional beam in the desired direction, the CG plays a more important role in increasing the SNR of the system. This becomes clear by looking at the beam pattern of the complete antenna array shown in Figure 5. The blue shaded area within the figure represents the range of all possible ζ_β. As a reference serves the ideal beam pattern obtained from simulation. The necessity of a calibration becomes obvious by measuring the beam pattern of the uncalibrated system shown in Figure 5(a). Due to the imbalances in amplitude and phase between the RF branches, the beam pattern is strongly distorted. The results for both optimization criteria indicate the beam points towards the desired spatial direction. Moreover, the optimization of the mean CG achieves an increased antenna array gain compared to the optimization of the phase error by 1.2 dB for $\phi = 0°$ and 2.2 dB for $\phi = -34°$ compared to the optimization of the phase error. The measured RMS sidelobe level over all steering angles result for both optimization criteria in 10.5 dB, which is only slightly below the simulated RMS sidelobe level of 11.4 dB.

To study the changes in receiver efficiency, the radiated power can be determined by integrating over the antenna pattern. As a reference, the radiated power averaged over all $\mathbf{N_p}$ phase shifter permutations

$$P_{\text{ref}} = \frac{1}{N_p} \sum_{p=1}^{N_p} \int \left| C_p(\phi) \right|^2 d\phi \tag{9}$$

can be calculated, where $C_p(\phi)$ represents the antenna pattern in azimuth of the pth selected permutation. The radiated power of the pth selected permutation results in

$$P_p = \int \left| C_p(\phi) \right|^2 d\phi. \tag{10}$$

By relating the optimization results to the reference P_{ref} using $(P_p - P_{\text{ref}})/P_{\text{ref}}$, an increase in radiated power of 14.8% is shown for phase optimization and 44.4% for amplitude optimization. This increment indicates a growth in the receiver efficiency due to the optimized selection of the phase states.

5. Conclusions

As described in this paper, the calibration of massive MIMO systems, consisting of hundreds of antenna elements, is a current challenge in industry and research. The classical calibration approach, using a separate calibration branch before or after each antenna element, is no longer realizable due to the dense packing and the large number of antenna elements. Therefore, an OTA calibration method based on scattering parameter measurements is proposed and evaluated using a novel SBHB receiver system operating at 27.8 GHz. The

correction of the phase and amplitude differences between the RF branches is performed by the employed phase shifters and variable attenuators within the SBHB RF-backend. To further improve the calibration result, two optimization criteria are formulated exploiting the phase shifter ambiguities. The results show that by optimizing the amplitude, the CG can be increased by 2.4 dB compared to the RMS value while ensuring a sufficiently low phase error of 6.3°. Thus, the measured beam pattern achieves approximately the performance of the results obtained by numerical simulations.

Data Availability

The data used to support the findings of this study are included within the article.

Conflicts of Interest

The authors declare that there are no conflicts of interest regarding the publication of this paper.

Acknowledgments

Many thanks are due to A. Lipp and A. Gallego for their support in assembling the SBHB receiver. Furthermore, we thank T. Bross from Richardson Electronics GmbH and A. Crofts from Anokiwave for their help with the utilized *AWMF-0108* SoC. This work was supported by the Electronic Components and Systems for European Leadership (ECSEL) joint undertaking funded under H2020-EU.2.1.1.7. in the frame of the TARANTO project with ID 737454 and the German Federal Ministry of Education and Research under grant number 16ESE0211.

References

[1] J. G. Andrews, S. Buzzi, W. Choi et al., "What will 5G be?," *IEEE Journal on Selected Areas in Communications*, vol. 32, no. 6, pp. 1065–1082, 2014.

[2] H. Viswanathan and M. Weldon, "The past, present, and future of mobile communications," *Bell Labs Technical Journal*, vol. 19, pp. 8–21, 2014.

[3] A. Swindlehurst, E. Ayanoglu, P. Heydari, and F. Capolino, "Millimeter-wave massive MIMO: the next wireless revolution?," *IEEE Communications Magazine*, vol. 52, no. 9, pp. 56–62, 2014.

[4] M. Xiao, S. Mumtaz, Y. Huang et al., "Millimeter wave communications for future mobile networks," *IEEE Journal on Selected Areas in Communications*, vol. 35, no. 9, pp. 1909–1935, 2017.

[5] B. Yang, Z. Yu, J. Lan, R. Zhang, J. Zhou, and W. Hong, "Digital beamforming-based massive MIMO transceiver for 5G millimeter-wave communications," *IEEE Transactions on Microwave Theory and Techniques*, vol. 66, no. 7, pp. 3403–3418, 2018.

[6] S. Han, I. Chih-lin, Z. Xu, and C. Rowell, "Large-scale antenna systems with hybrid analog and digital beamforming for millimeter wave 5G," *IEEE Communications Magazine*, vol. 53, no. 1, pp. 186–194, 2015.

[7] Y. J. Cho, G.-Y. Suk, B. Kim, D. K. Kim, and C.-B. Chae, "RF lens-embedded antenna array for mmWave MIMO: design and performance," *IEEE Communications Magazine*, vol. 56, no. 7, pp. 42–48, 2018.

[8] A. F. Molisch, V. V. Ratnam, S. Han et al., "Hybrid beamforming for massive MIMO: a survey," *IEEE Communications Magazine*, vol. 55, no. 9, pp. 134–141, 2017.

[9] F. Sohrabi and W. Yu, "Hybrid analog and digital beamforming for OFDM-based large-scale MIMO systems," in *2016 IEEE 17th International Workshop on Signal Processing Advances in Wireless Communications (SPAWC)*no. 978, pp. 1–5, Edinburgh, UK, 2016.

[10] R. W. Heath, N. Gonzalez-Prelcic, S. Rangan, W. Roh, and A. M. Sayeed, "An overview of signal processing techniques for millimeter wave MIMO systems," *IEEE Journal of Selected Topics in Signal Processing*, vol. 10, no. 3, pp. 436–453, 2016.

[11] W. Roh, J. Y. Seol, J. Park et al., "Millimeter-wave beamforming as an enabling technology for 5G cellular communications: theoretical feasibility and prototype results," *IEEE Communications Magazine*, vol. 52, no. 2, pp. 106–113, 2014.

[12] Y. Kim, H. Y. Lee, P. Hwang et al., "Feasibility of mobile cellular communications at millimeter wave frequency," *IEEE Journal of Selected Topics in Signal Processing*, vol. 10, no. 3, pp. 589–599, 2016.

[13] M.-Y. Huang, T. Chi, F. Wang, T.-W. Li, and H. Wang, "A 23-to-30GHz hybrid beamforming MIMO receiver array with closed-loop multistage front-end beamformers for full-FoV dynamic and autonomous unknown signal tracking and blocker rejection," in *IEEE international solid - state circuits conference - (ISSCC)*, vol. 61, pp. 68–70, San Francisco, CA, USA, 2018.

[14] X. Wei, Y. Jiang, and X. Wang, "Calibration of phase shifter network for hybrid beamforming in mmwave massive MIMO systems," in *ICC 2019 - 2019 IEEE International Conference on Communications (ICC)*, pp. 1–6, Shanghai, China, 2019.

[15] S. Hur, T. Kim, D. J. Love, J. V. Krogmeier, T. A. Thomas, and A. Ghosh, "Millimeter wave beamforming for wireless backhaul and access in small cell networks," *IEEE Transactions on Communications*, vol. 61, no. 10, pp. 4391–4403, 2013.

[16] A. Alkhateeb, O. El Ayach, G. Leus, and R. W. Heath, "Channel estimation and hybrid precoding for millimeter wave cellular systems," *IEEE Journal of Selected Topics in Signal Processing*, vol. 8, no. 5, pp. 831–846, 2014.

[17] S. Noh, M. D. Zoltowski, and D. J. Love, "Multi-resolution codebook and adaptive beamforming sequence design for millimeter wave beam alignment," *IEEE Transactions on Wireless Communications*, vol. 16, no. 9, pp. 5689–5701, 2017.

[18] Z. Xiao, T. He, P. Xia, and X. G. Xia, "Hierarchical codebook design for beamforming training in millimeter-wave communication," *IEEE Transactions on Wireless Communications*, vol. 15, no. 5, pp. 3380–3392, 2016.

[19] C. Lin, G. Y. Li, and L. Wang, "Subarray-based coordinated beamforming training for mmwave and sub-THz communications," *IEEE Journal on Selected Areas in Communications*, vol. 35, no. 9, pp. 2115–2126, 2017.

[20] M. Kokshoorn, H. Chen, P. Wang, Y. Li, and B. Vucetic, "Millimeter wave MIMO channel estimation using overlapped beam patterns and rate adaptation," *IEEE Transactions on Signal Processing*, vol. 65, no. 3, pp. 601–616, 2017.

[21] Y. Zhu, Q. Zhang, and T. Yang, "Low-complexity hybrid precoding with dynamic beam assignment in mmwave OFDM systems," *IEEE Transactions on Vehicular Technology*, vol. 67, no. 4, pp. 3685–3689, 2018.

[22] J. Eisenbeis, N. Kern, M. Tingulstad, L. de Oliveira, and T. Zwick, "Sparse array channel estimation for subarray-based hybrid beamforming systems," *IEEE Wireless Communications Letters*, p. 1, 2020.

[23] Y. Qi, G. Yang, L. Liu et al., "5G over-the-air measurement challenges: overview," *IEEE Transactions on Electromagnetic Compatibility*, vol. 59, no. 6, pp. 1661–1670, 2017.

[24] X. Wang, C. Yu, Y. Li, W. Hong, and A. Zhu, "Real-time single channel over-the-air data acquisition for digital predistortion of 5G massive MIMO wireless transmitters," in *2019 IEEE MTT-S International Wireless Symposium (IWS)*, pp. 1–3, Guangzhou, China, 2019.

[25] Y. Dong, S. Dong, Y. Wang, and L. Gong, "Calibration method of retrodirective antenna array for microwave power transmission," in *2013 IEEE Wireless Power Transfer (WPT)*, pp. 41–43, Perugia, Italy, 2013.

[26] L. J. Foged, L. Scialacqua, F. Saccardi, N. Gross, and A. Scannavini, "Over the air calibration of massive MIMO TDD arrays for 5G applications," in *2017 IEEE International Symposium on Antennas and Propagation & USNC/URSI National Radio Science Meeting*, pp. 1423-1424, San Diego, CA, USA, 2017.

[27] M. Jokinen, O. Kursu, N. Tervo, J. Saloranta, M. E. Leinonen, and A. Parssinen, "Over-the-air phase measurement and calibration method for 5G mmW phased array radio transceiver," in *2019 93rd ARFTG Microwave Measurement Conference (ARFTG)*, pp. 1–4, Boston, MA, USA, 2019.

[28] J. Eisenbeis, M. Tingulstad, N. Kern et al., "MIMO communication measurements in small cell scenarios at 28 GHz," IEEE Transactions on Antennas and Propagation, 2020.

[29] Anokiwave, *Preliminary Data Sheet - Ka-Band Silicon 5G Quad Core IC - AWMF-0108*, Anokiwave, 2017, https://www.anokiwave.com/#.

[30] R. Rotman, M. Tur, and L. Yaron, "True time delay in phased arrays," *Proceedings of the IEEE*, vol. 104, no. 3, pp. 504–518, 2016.

[31] C. A. Balanis, *Antenna Theory: Analysis and Design*, Wiley, 2015.